

Article

Investigation of Time-Varying Cable Tension of Bridges Using Time-Frequency Reassignment Techniques Based on Structural Health Monitoring Data

Maosen Cao ¹, Shuaitao Hu ¹, Xin Zhang ^{1,*} , Shixiang Zhang ², Dragoslav Sumarac ³ and Jiayi Peng ^{1,4}

¹ College of Mechanics and Materials, Hohai University, Nanjing 210098, China; cmszhy@hhu.edu.cn (M.C.); hst@hhu.edu.cn (S.H.); pjy50@jsti.com (J.P.)

² Jiangsu Key Laboratory of Intelligent Perception and Control of Integrated Transportation, China Design Group Co., Ltd., Nanjing 210014, China; 13505197324@163.com

³ Faculty of Civil Engineering, University of Belgrade, 11000 Belgrade, Serbia; dragosumi@gmail.com

⁴ The State Key Laboratory for the Safety and Health of Long-Span Bridges in Service, Jiangsu Transportation Research Institute, Nanjing 211100, China

* Correspondence: xzhang@hhu.edu.cn

Featured Application: The method proposed in this paper can quickly identify the time-varying cable tension and have the potential for condition monitoring and performance evaluation of cables under special events, such as typhoons, earthquakes and heavy traffic.

Abstract: Cables have been increasingly utilized in modern long-span or tied-arch bridges as the main bearing structures. Real-time identification of time-varying cable tension is essential for assessing the service performance of bridges. Vibration-based methods have been an increasing research focus in recent decades. However, a long time interval is needed to estimate structural frequency using vibration-based methods, increasing the calculating time of cable tension. The time-varying cable tension is thus difficult to extract. This study proposes a time-frequency reassignment-based algorithm to reduce the detection time to address this issue. Combined with a time-frequency analysis tool and vibration theory of cables, the algorithm can identify the time-varying frequency and further quickly calculate the time-varying cable tension within 12.8 s. The features of the proposed algorithm are mainly threefold: identifying the time-varying frequencies with high precision; without some prior knowledge of vibration; having no other requirements for sensor modes. Moreover, the experimental validation is conducted using a quasi-static loading in a workshop and a dynamic field test on Sutong Bridge, respectively. The results show that the proposed algorithm can be used to identify time-varying tension and assess the service performance of cables, providing a new path for real-time condition monitoring of bridges in service.

Keywords: cable tension; dynamic responses; time-frequency reassignment; field experiment; structural health monitoring



Citation: Cao, M.; Hu, S.; Zhang, X.; Zhang, S.; Sumarac, D.; Peng, J. Investigation of Time-Varying Cable Tension of Bridges Using Time-Frequency Reassignment Techniques Based on Structural Health Monitoring Data. *Appl. Sci.* **2022**, *12*, 4008. <https://doi.org/10.3390/app12084008>

Academic Editors: Werner Lienhart and M. Shamim Miah

Received: 14 March 2022

Accepted: 12 April 2022

Published: 15 April 2022

Publisher's Note: MDPI stays neutral with regard to jurisdictional claims in published maps and institutional affiliations.



Copyright: © 2022 by the authors. Licensee MDPI, Basel, Switzerland. This article is an open access article distributed under the terms and conditions of the Creative Commons Attribution (CC BY) license (<https://creativecommons.org/licenses/by/4.0/>).

1. Introduction

As the main load bearing structures, cables have been widely used in many long-span bridges or large-scale space buildings in recent decades due to their superb material properties, low costs and advanced design theories [1–5]. However, unfavorable factors, such as environmental erosion and fatigue loads do inevitably result in damage, including corrosion, abrasion, fatigue crack, or broken wire [6–10]. The accumulation of damage can weaken the service performance, bringing potential hazards and may cause a serious accident. Therefore, condition monitoring of cables plays an important role in keeping the integrity of entire structures [11–14].

Tension is a straightforward and key parameter to assess the operating conditions of cables. Currently, various structural health monitoring (SHM) methods are applied

to identify the cable tension, including the load cell method [15], fiber Bragg grating method [16,17], elasto-magnetic method [18], elasto-magneto-electric method [19], and vibration-based method. The load cell and fiber Bragg grating method need to be pre-installed and calibrated during the construction stage and can online measure the tension with high precision. However, the reliability will gradually decrease over time due to sensor debonding or biological bite damage. The elasto-magnetic method can be used to measure the tension and detect the broken wire damage of cables. However, the test equipment is relatively expensive, and the method is time-consuming during the excitation process. The elasto-magneto-electric method is an emerging method with significant advantages in identifying cable tension, but it has high requirements for measurement conditions (e.g., stationary temperature and humidity). Among the above evaluation methods, vibration-based methods have been proven as cost-effective in tension identification due to the advantages of explicit mechanical formulation, facilitation in acquiring dynamic response, and abundant application cases [20–22]. The foundation of this method is according to vibration theory which represents the physical relationship between tension and vibration frequency [23–27]. Many studies clarify this relationship in various models by considering the effect of sag, inclination, or bending stiffness [27–29]. In particular, structural frequencies can be identified by the measured dynamic responses such as acceleration. Afterward, the cable tension can be indirectly calculated using structural frequencies based on the mechanical models.

Generally, the vibration-based method requires a sampling interval for frequency identification via some time-frequency analysis tools such as the Fourier transform (FT). The cable tension is supposed to be a constant during this time interval. However, in practical engineering, cable tension is associated with the variation of loads and thus is a time-varying parameter under different operating conditions. The time-varying cable tension is an important indication and thus is the main concern of bridge management departments. Therefore, to reflect the time-varying tension, the measurement interval for frequency identification should be made as soon as possible, i.e., the time-varying instantaneous frequency of structures is necessary.

To approach this purpose, many existing studies have been focused on identifying the time-varying instantaneous frequency of cables, including the extended Kalman filter [30], complexity pursuit [31], adaptive sparse time-frequency analysis [32], an extended analytical mode decomposition-Hilbert transform-zoom synchrosqueezing wavelet transform combined method [33], conjugate-pair decomposition [34], and variational mode decomposition [35]. In particular, the extended Kalman filter-based method is firstly proposed to address the key problem of time-varying tension identification in the research field. The effectiveness of the method is verified by both numerical examples and experimental verification in the laboratory. Then, the complexity pursuit algorithm can also identify the time-varying tension with high accuracy but requires at least two acceleration sensors to implement the process of independent component analysis. Next, the adaptive sparse time-frequency analysis is used to identify the time-varying tension, yet the initial phase of vibration should be determined before time-frequency analysis. Moreover, the mentioned combined method can identify the time-varying first order frequency and further calculate the tension with excellent results, although the algorithm has a complex identification process in dealing with a narrowband signal. In addition, the effectiveness of the conjugate-pair decomposition is proved by the numerical examples, but still needs further experimental verification in the future. Finally, the variational mode decomposition can extract the instantaneous change of cable tension with acceptable results. However, the number of decomposition layers is an artificial setting parameter that impacts the identification results.

The time-varying instantaneous tension is well identified using the above methods with both numerical and experimental verification. However, these methods are only applied in the laboratory and lack a field experiment verification in practical engineering. Meanwhile, the identified time-varying tension is not used to evaluate the operating

conditions of cables in bridge engineering. Therefore, it is essential to develop a method to real-time identify the cable tension and assess the service performance of cables in practical bridge engineering.

This study proposes a time-frequency reassignment (TFR)-based algorithm for identifying time-varying cable tension. The proposed algorithm, combined with a time-frequency analysis tool and the vibration theory of cables, can identify the time-varying instantaneous frequency and further calculate the time-varying cable tension with satisfactory results. Compared with existing methods, this work is a different attempt, especially focusing on the applicability of the algorithms to practical engineering. The main innovation of the proposed algorithm lies in three parts: (a) the reassignment operator can give the algorithm the ability to identify the time-varying frequencies with high precision; (b) the algorithm is developed without some prior knowledge of vibration; (c) the application of the algorithm is verified using concrete engineering tests and have no other requirements on sensor modes. One accelerometer is enough for the implementation of the proposed algorithm.

The rest of the paper is organized as follows: Section 2 briefly introduces the basic theory and features of TFR. Section 3 formulates an identification algorithm with a concrete implementation process. Section 4 experimentally demonstrates the algorithm through a large-scale cable with loading and unloading tests in a workshop. Section 5 further investigates the proposed algorithm for practical bridge engineering using an in situ field experiment. The service performance of the measured cable is also evaluated using the identified time-varying tension. Section 6 presents the conclusions of this study.

2. TFR Techniques

2.1. Short-Time Fourier Transform

Without loss of generality, it is supposed that an integrable multi-component signal can be expressed as:

$$s(t) = \sum_{k=1}^n s_k(t), \quad (1)$$

$$s_k(t) = A_k(t)e^{i\phi_k(t)}, \quad (2)$$

where $A_k(t)$ and $\phi_k(t)$ are the amplitude and phase function of $s_k(t)$, respectively. In order to extract local time-frequency characteristics $A_k(t)$ and $\phi_k(t)$, short-time Fourier transform (STFT) has been utilized broadly in various scientific fields. The STFT of a signal $s(t)$ is defined as [36]

$$F_s^g(t, \omega) = \int_R s(\tau)g^*(\tau - t)e^{-i\omega\tau}d\tau, \quad (3)$$

where $g(t)$ is the window function, $g^*(t)$ is the complex conjugate of $g(t)$. The parameters t and ω are the time and frequency variables, respectively. Afterward, the time-frequency spectrogram $P_s^g(t, \omega)$ is then defined as

$$P_s^g(t, \omega) = \left| F_s^g(t, \omega) \right|^2. \quad (4)$$

2.2. Uncertainty Principle

The significant issue in signal processing is the uncertainty principle, also named the Heisenberg–Gabor limit, which clarifies that one cannot simultaneously localize a signal with an arbitrary precision both in the time and frequency domains. There is a trade-off between the time resolution and frequency resolution depending on a key control parameter, e.g., the length of window function $g(t)$ in STFT. In other words, it is difficult to identify the frequency in a concise time interval because the frequency resolution is relatively low under these conditions.

Many time-frequency analysis tools are proposed to address this trade-off problem, such as quadratic representations using the Wigner–Ville distribution (WVD) [37] or other

autoregressive methods [38]. The frequency resolution is improved using these methods but may produce undesirable artifacts.

2.3. Time-Frequency Analysis Using TFR

TFR techniques offer another approach to sharpening the time-frequency representation while keeping the temporal localization and can extract improved frequency resolution [39,40]. Based on the STFT frame, the implementation process is as follows.

First, the spectrogram $P_s^g(t, \omega)$ of signals can also be expressed as

$$P_s^g(t, \omega) = \iint_{\mathbb{R}^2} W_s(\tau, v) W_g(\tau - t, v - \omega) \frac{d\tau dv}{2\pi}, \tag{5}$$

where W_s and W_g are the WVD of signal $s(t)$ and window function $g(t)$, defined as the FT of instantaneous correlation function:

$$W_s(t, \omega) = \int_{\mathbb{R}} s\left(t + \frac{\pi}{2}\right) s^*\left(t - \frac{\pi}{2}\right) e^{-i\omega\tau} d\tau, \tag{6}$$

WVD can reflect the instantaneous time-frequency relationship of the signal, especially for a single component signal. However, the quadratic representations may produce cross-term interference for multi-component signals. Therefore, the spectrogram function is thus the two-dimensional smoothing function to reduce adverse effects. Then, the reassignment method is used to redefine the time-frequency spectrogram $P_s^g(t, \omega)$ based on the principle of centroid distribution:

$$\bar{P}_s^g(t, \omega) = \iint_{\mathbb{R}^2} P_s^g(t, \omega) \delta(\omega - \omega_s(\tau, v)) \delta(t - t_s(\tau, v)) d\tau dv, \tag{7}$$

where $\bar{P}_s^g(t, \omega)$ is the reassignment spectrogram of a signal $s(t)$. $\omega_s(\tau, v)$ and $t_s(\tau, v)$ are calculated by

$$\omega_s(\tau, v) = \omega - \text{Im} \left[\frac{F_s^{g'}(t, \omega)}{F_s^g(t, \omega)} \right], t_s(\tau, v) = t + \text{Re} \left[\frac{F_s^{tg}(t, \omega)}{F_s^g(t, \omega)} \right], \tag{8}$$

where g' is the derivative of the window function $g(t)$ and tg represents the factor $t \cdot g(t)$.

Based on Equations (7) and (8), the energy is reassigned in the time-frequency plane. Thus, the local time-frequency characteristic is easy to follow from the reassignment spectrogram $\bar{P}_s^g(t, \omega)$. The TFR techniques provide a new approach to identifying the time-varying frequency, particularly well adapted to multi-component signals.

3. Identification of Cable Tension Using TFR Techniques

3.1. Dynamic Response of Cables

Generally, structural deflection can be divided into several modal shapes that correspond to each natural frequency [41]. The modal shapes are deflection conditions of free vibration. The higher-order mode shape is pretty low and can be ignored. Therefore, the first N order modal shapes can determine the whole vibration characteristics of structural dynamic responses.

Without loss of generality, the in-plane acceleration response of a uniform cable can be expressed as

$$a_{x_0}(t) = \sum_{k=1}^M \varphi_k^{x_0} \sin(2\pi f_k t + \mu_k), \tag{9}$$

where x_0 , $\varphi_k^{x_0}$, f_k , and μ_k are installation position of sensors, amplitude, frequency and phase of the k -th modal shape, respectively.

It can be seen from Equation (9) that the measured dynamic response can be regarded as a superposition of different modal shapes. The acceleration signal is thus a multi-

component signal consistent with the assumptions of Equation (1). In particular, according to string theory or other modified models, the higher-order frequencies are multiples of the fundamental frequency with small corrections. Therefore, the TFR technique is very suitable to solve the problem of time-frequency analysis for the vibration signals of cables, which is the original intention of this study.

3.2. Identification of Time-Varying Frequency

To identify the structural time-varying frequency of multi-component signals, the acceleration responses are then processed using TFR techniques. Firstly, the STFT of the acceleration signal is given by

$$F_a^g(t, \omega) = \int_R a_{x_0}(\tau) g^*(\tau - t) e^{-i\omega\tau} d\tau, \quad (10)$$

where the Gaussian window function is used in this study.

Then, it does not need to calculate the WVD of acceleration response. Based on the discussion in Section 2.3, three STFTs can be used to estimate the centroid frequency and calculate the time-frequency spectrogram $P_a^g(t, \omega)$ according to Equations (4) and (8). In the process of STFT, a suit length of the window function $g(t)$ should be determined by a parameter study.

Finally, the reassignment spectrogram $\bar{P}_a^g(t, \omega)$ of acceleration is rewritten as

$$\bar{P}_a^g(t, \omega) = \iint_{\mathbb{R}^2} P_a^g(t, \omega) \delta(\omega - \omega_a(\tau, v)) \delta(t - t_a(\tau, v)) d\tau dv, \quad (11)$$

where $\omega_a(\tau, v)$ and $t_a(\tau, v)$ are calculated by Equations (3) and (8). The reassignment spectrogram $\bar{P}_a^g(t, \omega)$ provides sharp time-frequency characteristics of the measured signals.

3.3. Identification of Time-Varying Cable Tension

Based on the results of the reassignment spectrogram $\bar{P}_a^g(t, \omega)$, the time-varying frequencies of cables are identified with the following process: First, the time-varying frequency on each sampling point j is picked up from the peak value point, where N is the number of the sampling points. Subsequently, the basic material parameters of the cable, such as length, mass per unit length, etc., need to be tested or referred to in the design data. Finally, the cable tension can be identified via measured frequency based on the relationship between the tension and frequency. Particularly, the string theory is used to calculate the tension in this study:

$$T = 4mL^2 \frac{f_k^j{}^2}{k^2} \quad (k = 1, 2, \dots, \infty), \quad (12)$$

where T , m , L , f_k^j , and k are taut tension, mass per unit length, length, the k -th frequency of sampling point j , and frequency order of the cable, respectively. In Equation (12), m and L are constant parameters for specific cables. Thus, cable tension T can be explicitly represented as a function with respect to f_k^j and k .

The detailed implementation process of the TFR-based algorithm is combined with the signal processing theory and mechanics theory. The identification algorithm can be divided into several steps, as shown in Figure 1.

- Step 1: Measure the dynamic response of cables from health monitoring systems;
- Step 2: Choose a suitable length of the window function $g(t)$, calculate three STFT spectrograms $F_a^g(t, \omega)$, $F_a^{g'}(t, \omega)$, and $F_a^{tg}(t, \omega)$;
- Step 3: Calculate the time-frequency reassignment spectrogram $\bar{P}_a^g(t, \omega)$ from three STFTs and compare the time-frequency resolution using the different length of window function in parameter studies;

Step 4: Identify the time-varying frequency from the reassignment spectrogram $\bar{P}_a^g(t, \omega)$ by picking the peak ridge;
 Step 5: Calculate the time-varying tension based on the vibration theory of cables by Equation (12).

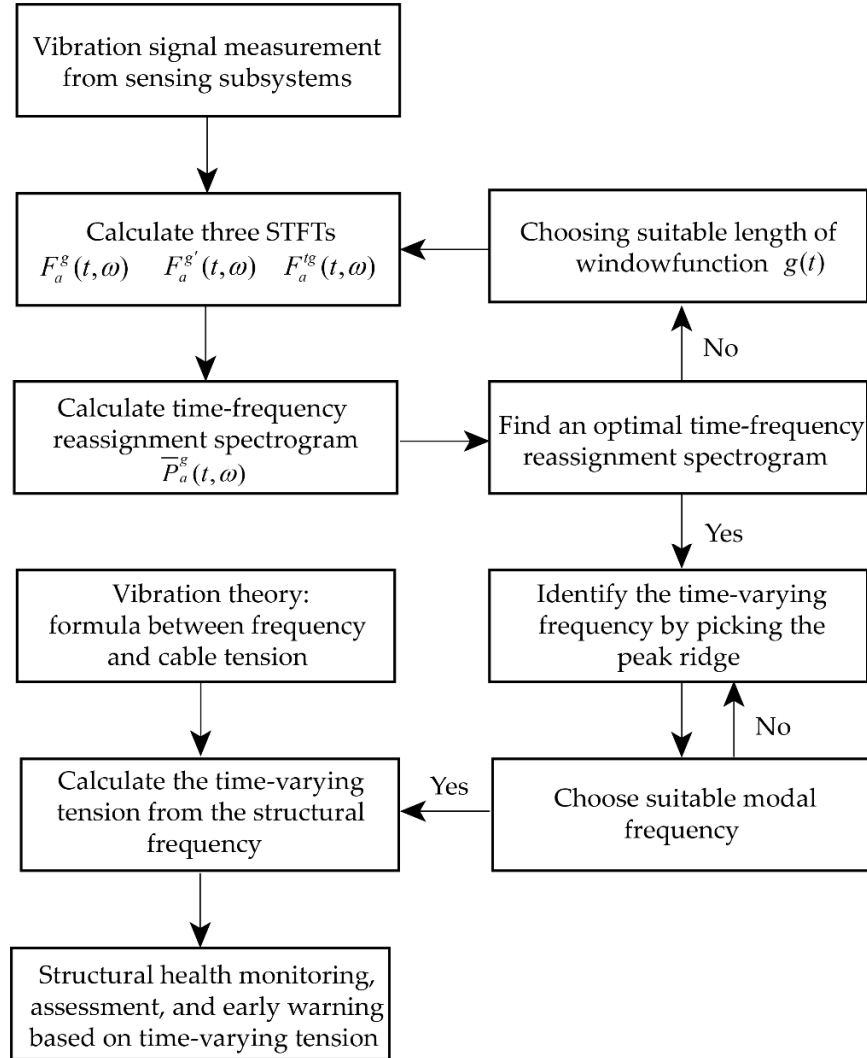


Figure 1. Algorithm flow of identification of time-varying cable tension based on TFR.

4. Experimental Validation

4.1. Experimental Descriptions

The proposed tension identification algorithm, based on TFR techniques, was verified experimentally using a workshop test. A cable of parallel steel wires was prepared in the test pit as the experimental sample, as shown in Figure 2. The experimental cable consists of 127 steel wires with a diameter of 5.2 mm per each and a double protective layer made of polyethylene, as shown in Figure 3. The length and mass per unit length of the experimental cable are 191.9 m and 22 kg/m, respectively. The detailed parameters of cables are shown in Table 1. The structural system had one fixed end and one end connected with a hydraulic jack. Several rubber rollers were placed under the cable to prevent it from being broken at low-level loads.

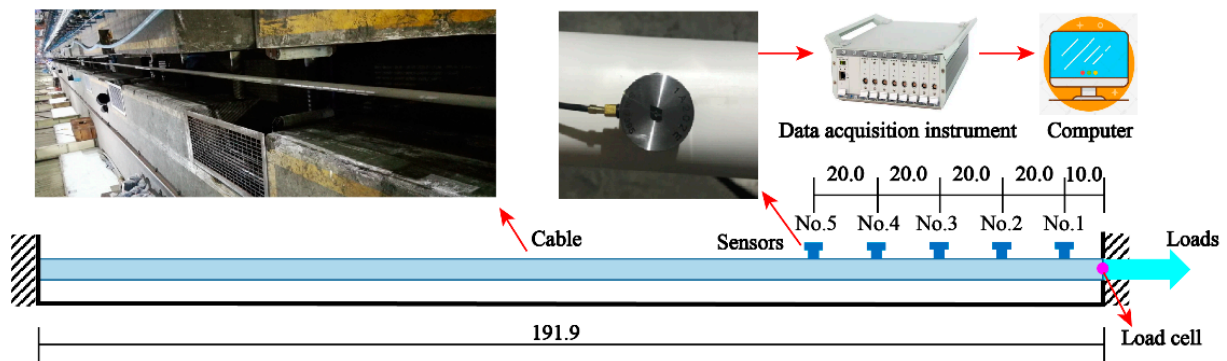


Figure 2. Experimental set-up.

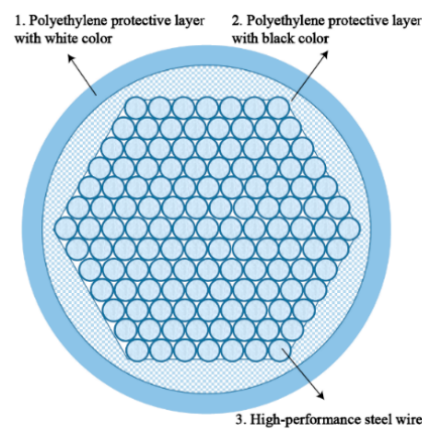


Figure 3. Cross-section details of experimental cable.

Table 1. Parameters of the experimental cable.

Length (m)	Mass per Unit (kg/m)	Specification (mm)	Anchorage Length (m)	Protective Sleeve Material
191.9	22.0	127 × Φ5.2	1.0	Polyethylene

4.2. Data Acquisition

The data acquisition and assessment systems consist of five accelerometers, a load cell, a data acquisition instrument, and a computer, as shown in Figure 2. The DH-1A202E voltage output accelerometers were adopted in the experiment. The accelerometers have the characteristics of a no zero offset and strong anti-interference ability, which is suitable to measure low-frequency vibration. The sampling frequency, measuring range, sensitivity, dimensions and weight of the accelerometers are 20 Hz, 50 m·s⁻², 10 mV/m·s⁻², Φ31.5 × 34 mm and 172 g, respectively. Meanwhile, a load cell was installed on the hydraulic jack, and the sampling frequency of the load cell is 1 Hz. The detailed layout of the sensors is shown in Figure 2. Five accelerometers were installed 10 m away from the loading side, with a space of 20 m. The data acquisition instrument converted the voltage signals into digital signals and then saved them in the computer for analysis.

The loading process of the experiment was divided into three stages: loading, slow unloading, and fast unloading. The loading force was measured by the load cell, as shown in Figure 4. Firstly, the longitudinal loading tension increased gradually from 2255.8 kN to 2458.1 kN in 27 s. Then, the loading tension decreased with a slow unloading speed from 2458.1 kN to 2450.3 kN in 135 s. Finally, the loads drop rapidly to 2305.9 kN in 17 s.

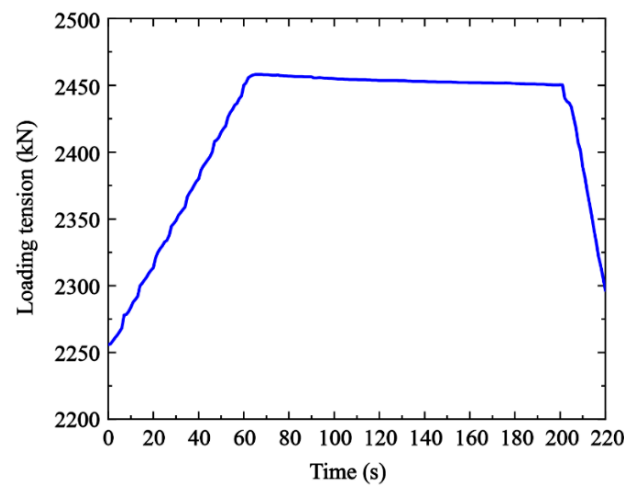


Figure 4. Loading tension measured by the load cell.

Using the accelerometers, the in-plane dynamic responses of the cable were collected, as shown in Figure 5. Except for the loads and environment noise, no other excitation force was applied to the structural system. Therefore, the acceleration conforms to free vibration with the amplitude of gradual attenuation.

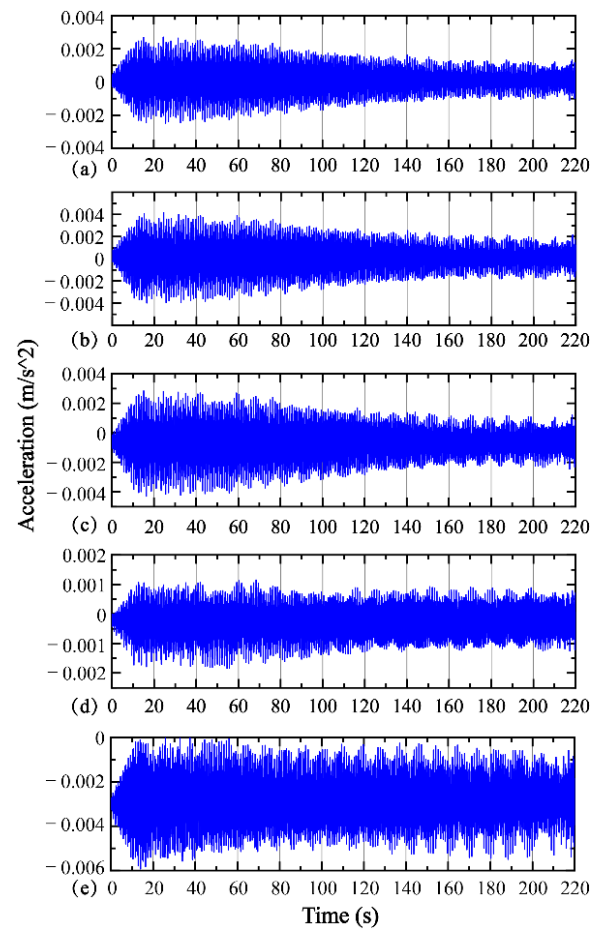


Figure 5. Acceleration of the cables by (a) Sensor 1, (b) Sensor 2, (c) Sensor 3, (d) Sensor 4, and (e) Sensor 5.

4.3. Results

4.3.1. Optimal Selection of Window Function Length

The length of the window function is an optional parameter in the TFR frame. Generally, the sampling point is selected as the n^{th} power of 2 in order to ensure the convenience of the algorithm. In order to find an optimal window length, the time-frequency reassignment spectrogram $\overline{P}_a^S(t, \omega)$ is calculated by different lengths, such as 64, 128, 256, and 512, corresponding to the sampling intervals 3.2 s, 6.4 s, 12.8 s, and 25.6 s, as shown in Figure 6. It is obvious to see from the figure that the time-frequency resolution of length 64 is very low, hard to extract the frequency along the time axis. The resolution becomes better when using 128 sampling points, but still represents a zigzag fluctuation in the time-frequency spectrogram, especially in the low-frequency region. Hence, the time-frequency resolutions of 256 and 512 are much preferable to the previous results. Therefore, the length of the window function is chosen as 256 in the time-frequency analysis.

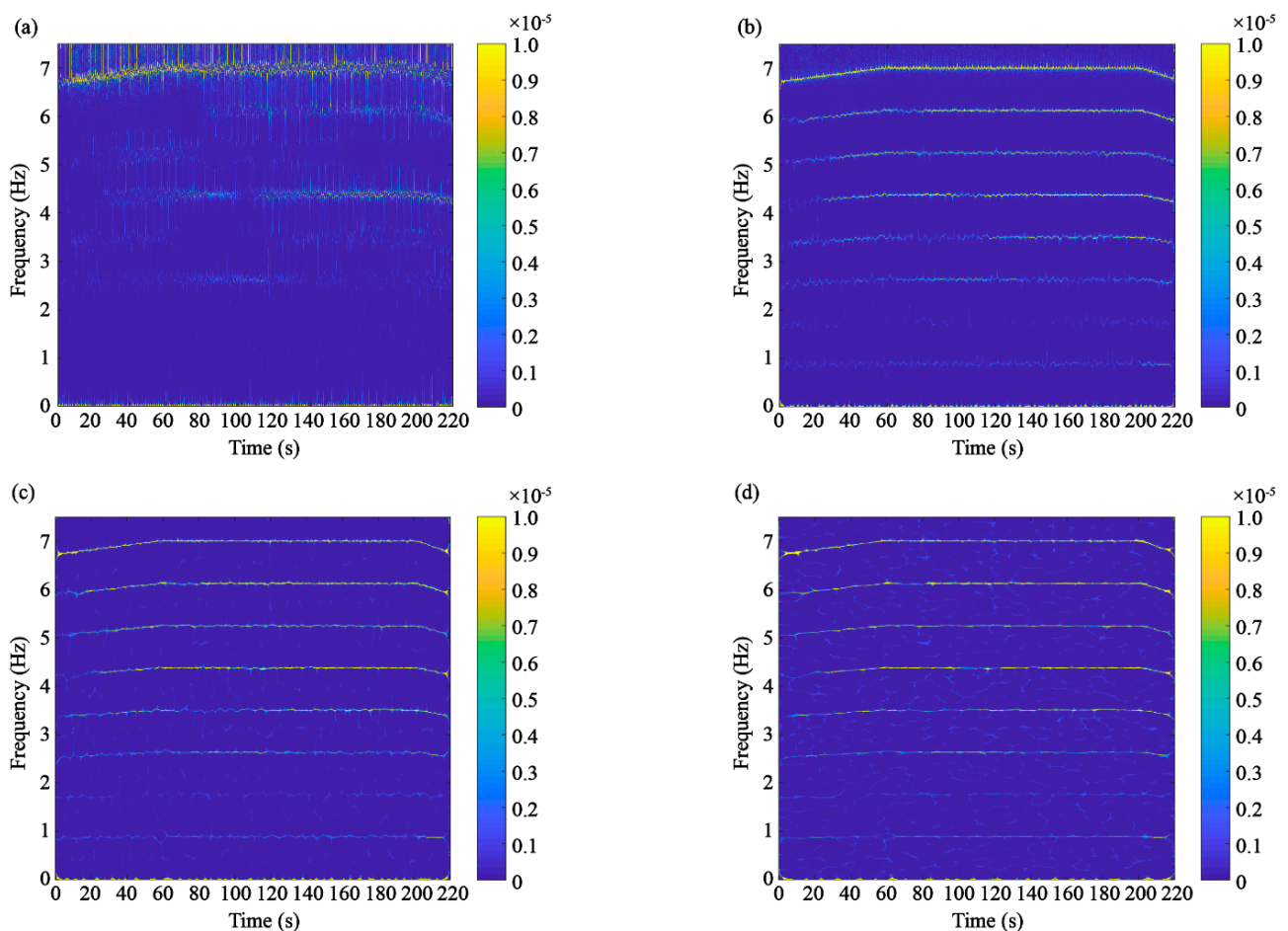


Figure 6. Time-frequency reassignment spectrogram with window function length of (a) 64, (b) 128, (c) 256, and (d) 512, respectively.

4.3.2. Time-Varying Frequency Extract Based on TFR

The TFR-based algorithm is implemented for the identification of cable tension based on measured acceleration responses. Firstly, the reassignment spectrograms of acceleration responses are shown in Figure 7. The window function length used in STFT is 256 based on the discussion in Section 4.3.1. It is obvious to see from Figure 7a that the first eight order frequencies are identified in the time-frequency plane. The energy of the 1st and 2nd order modal shapes is relatively low and almost unrecognizable. The zoom-in views of each sensor are shown in Figure 7b–f, respectively. The overall variation of frequencies is relatively consistent, corresponding to the loading process step by step.

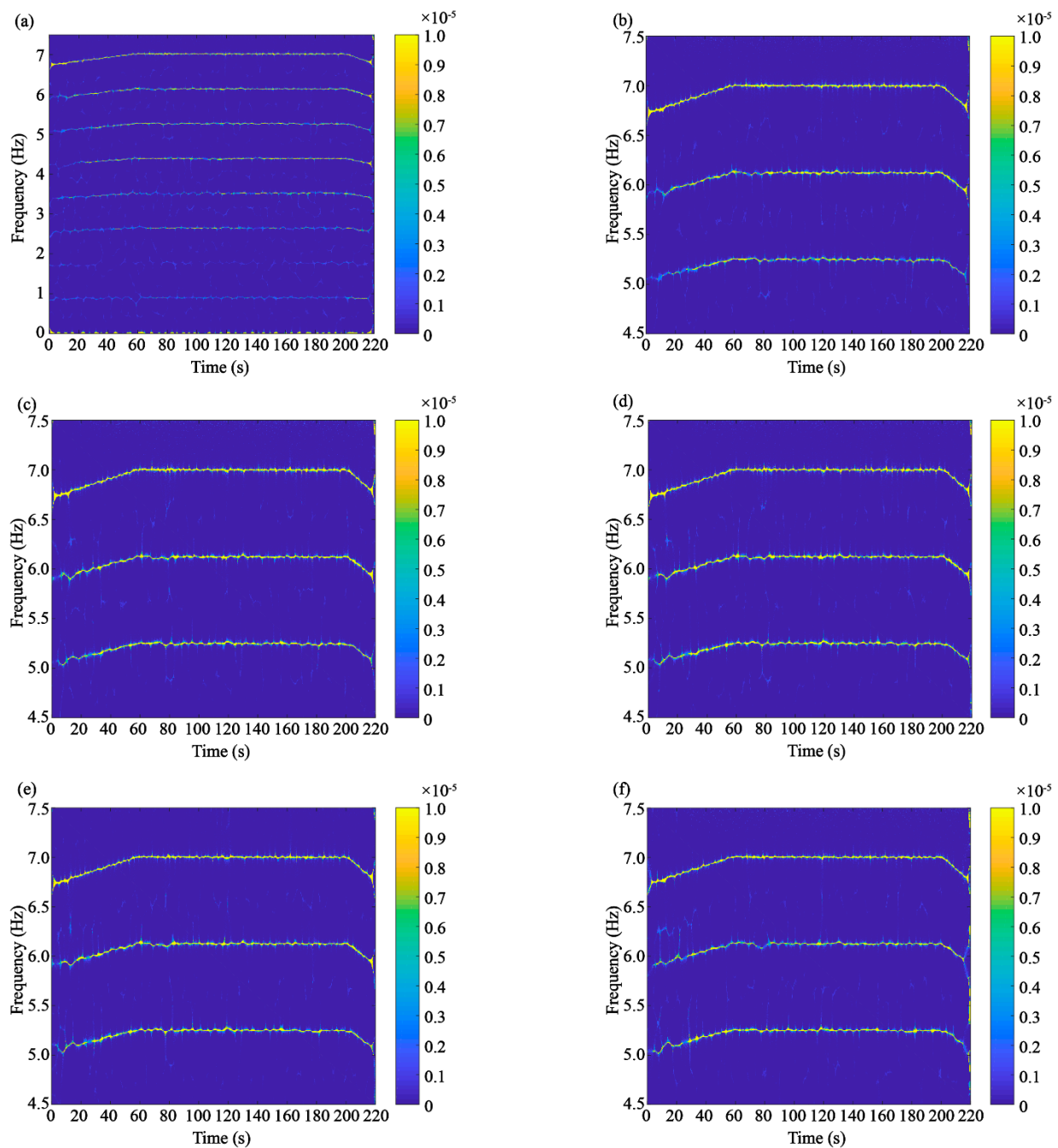


Figure 7. TFR spectrogram of measured acceleration response. (a) Sensor 1-global view, (b) Sensor 1 (c) Sensor 2, (d) Sensor 3, (e) Sensor 4, (f) Sensor 5-zoom-in view.

For comparison, traditional STFT analysis is also applied to deal with the acceleration signals. The STFT result is shown in Figure 8. The window function with the length of 256 sampling points, i.e., a time interval of 12.8 s, was used to extract the time-frequency characteristics simultaneously in the STFT frame. However, as mentioned in the introduction, the frequency resolution is pretty low if the length of the window function is short. Obviously, the time-frequency resolution is not as clear as the TFR-based algorithm shown in Figure 7. There is strong interference on the spectrum in Figure 8, so it can only roughly find the range of frequency distribution.

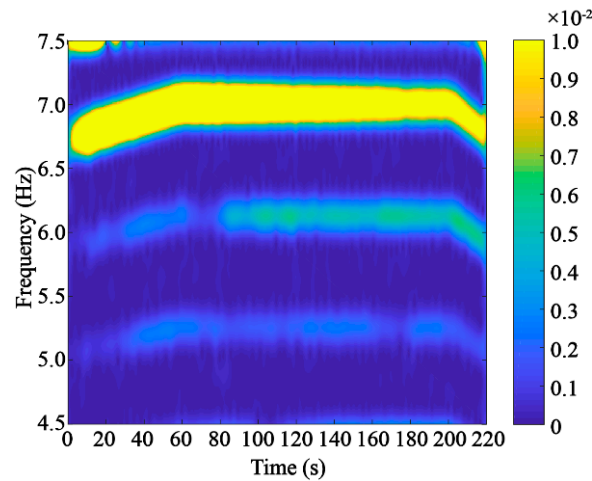


Figure 8. STFT of measured acceleration response by Sensor 1.

4.3.3. Time-Varying Cable Tension and Error Analysis

The proposed algorithm then processed the identified 4th to 8th frequencies to calculate the tension by Equation (12). The results are shown in Figure 9a. By comparison, the actual loads are also marked with red color in Figure 9a. The tension calculated by the low-order frequencies changes more than the higher-order frequencies. Meanwhile, each sensor identified the tension using the 8th order frequency, as shown in Figure 9b. Almost all the sensors get the same results and are close to the actual loads.

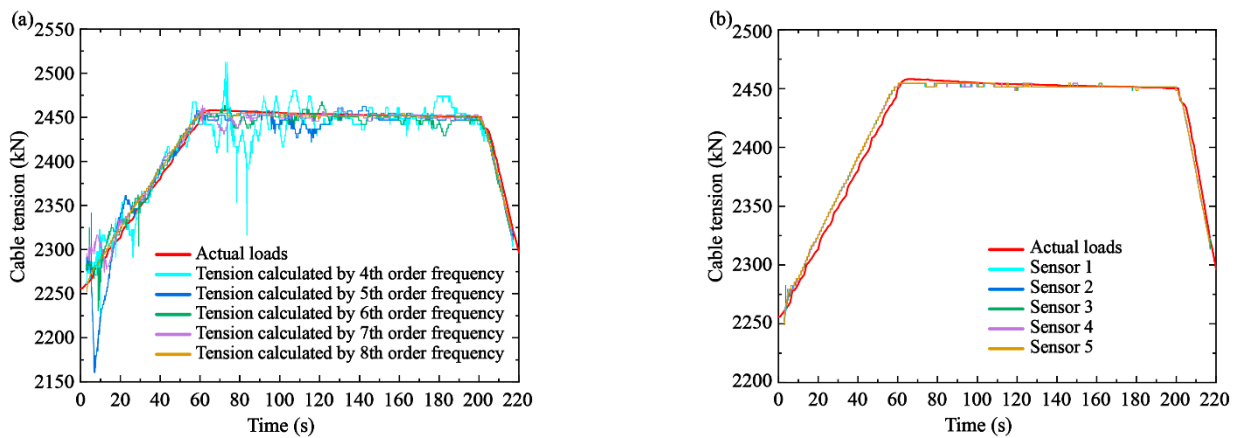


Figure 9. Identified tension compared with actual tension. (a) Identified tension using Sensor 1 with different frequencies and (b) identified tension using 8th order frequency with different sensors.

Moreover, the average error (AE) and maximum error (ME) are shown in Table 2 and Figure 10. The definitions of the errors can be expressed as

$$AE = \left(\frac{1}{N} \sum_{j=1}^N \frac{|T_{i,j} - T_{a,j}|}{T_{a,j}} \right) \times 100\%, \tag{13}$$

$$ME = \max_{j=1,2,\dots,N} \frac{|T_{i,j} - T_{a,j}|}{T_{a,j}} \times 100\%, \tag{14}$$

where j is the sampling points varying from 1 to N . It can be seen from Table 2 and Figure 10 that the AE of the TFR-based algorithm is between 0.16% to 0.59%, while the ME within 5.70% usually appears at the boundary of the signals or calculated results by the low-order frequencies (e.g., 4th order result marked with cyan color in Figure 9a). The error of higher-

order frequency is lower than that of low-order frequency. Almost all the ME are within 5%, which is in accord with the application requirements in engineering.

Table 2. Error of tension calculated by each order frequencies.

Frequency Order	Error	Sensor 1	Sensor 2	Sensor 3	Sensor 4	Sensor 5
4	AE (%)	0.51	0.49	0.44	0.47	0.59
	ME (%)	5.70	5.16	2.49	3.10	5.06
5	AE (%)	0.40	0.42	0.42	0.40	0.38
	ME (%)	5.16	4.95	4.95	4.78	5.04
6	AE (%)	0.27	0.29	0.29	0.28	0.30
	ME (%)	2.68	2.68	2.68	3.14	2.32
7	AE (%)	0.27	0.27	0.25	0.25	0.28
	ME (%)	1.82	1.88	2.16	1.37	3.43
8	AE (%)	0.16	0.17	0.16	0.17	0.17
	ME (%)	0.62	0.89	0.60	0.60	0.62

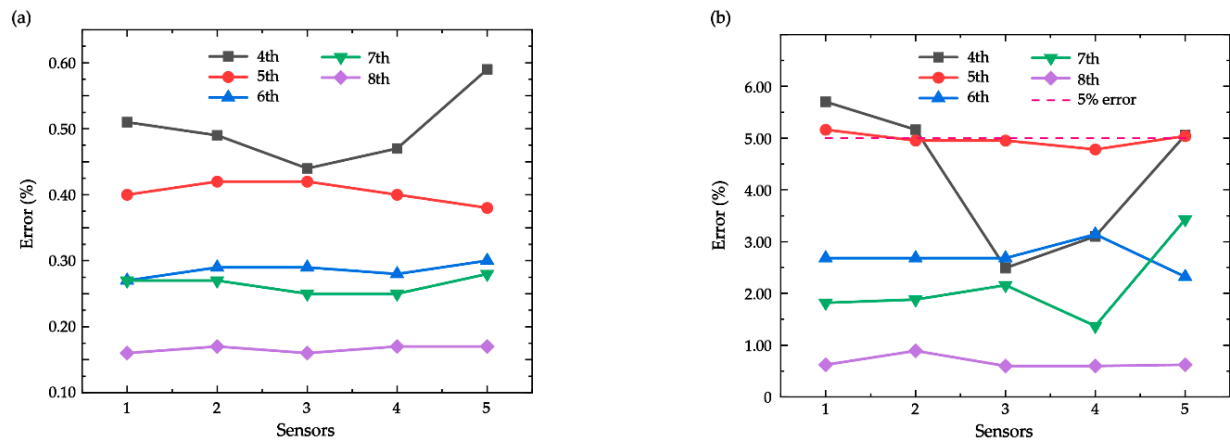


Figure 10. (a) Average error and (b) maximum error of each sensor.

5. Engineering Validation

5.1. Experiment Descriptions

To further verify the proposed TFR-based algorithm, a field experiment was designed and carried out on Sutong Bridge, a long-span cable-stayed bridge with 272 cables. This bridge locates at the entrance of the Yangtze River in China, connecting two cities Nantong and Suzhou. The main girder consists of three spans with lengths of 500 m + 1088 m + 500 m, as shown in Figure 11. The height of the tower is about 300 m.



Figure 11. Overview of the experimental bridge.

A special cable A18 in the south side span (downstream side) was chosen as the experimental object, as re-marked with red color in Figure 12. Specifically, the length and

mass per unit length of the cable are 336.811 m and 77.70 kg/m, respectively. These cable parameters were measured in the construction stage [42]. The experimental cable connects the tower and the main girder at the auxiliary pier. A series of strain gauges have also been installed at the bottom of the cable. The measured stress is a reference to validate the proposed method.

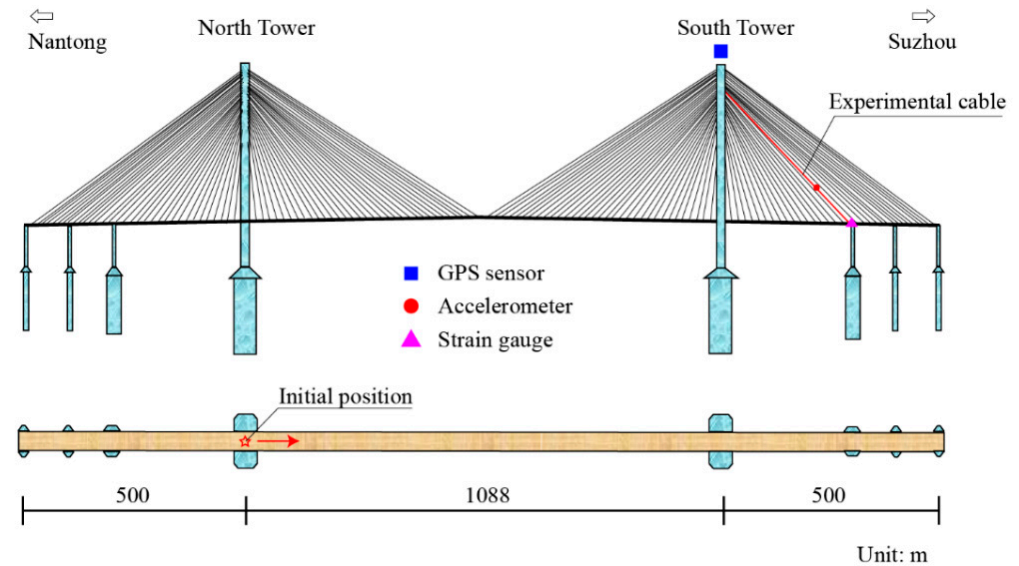


Figure 12. Basic information on the experimental bridge and sensors.

In contrast to the loading experiment in the workshop, the moving loads were adopted in the field experiment instead of the static loads. The photograph of the loading trucks is shown in Figure 13. In particular, four trucks full of sand and stones were used as applied loads in the dynamic test. The trucks started from the North Tower and moved towards the South Tower at a constant designed speed of 30 km/h (Case 1) and 40 km/h (Case 2), respectively.



Figure 13. Loading trucks in the field experiment.

5.2. Data Acquisition from Sensing Subsystem

Structural health monitoring systems were installed on the bridge for about ten years. From the sensing subsystems, the dynamic responses of cables and the main structure were measured by sensors. The type of accelerometer is the same as that in the workshop test. An accelerometer was installed near the 1/3 location of the cable. The sampling frequency of the accelerometer is 20 Hz. The measured acceleration response of the cable is shown in Figure 14.

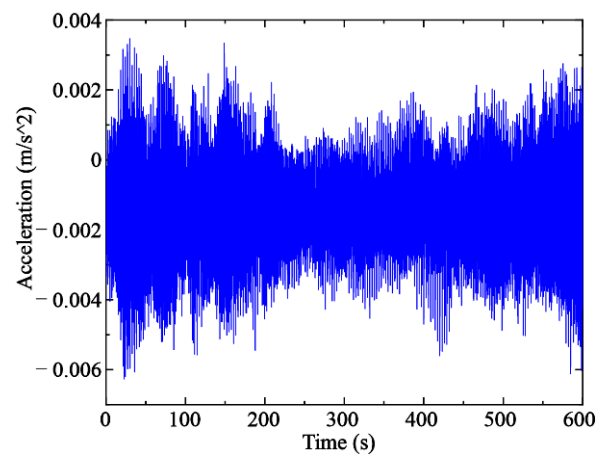


Figure 14. Acceleration of the experimental cable.

Limited to the in-service conditions, it is difficult to install a load cell or other sensors on the cable to acquire the cable tension directly. In this situation, a GPS sensor and a strain gauge were installed on the top of the South Tower and the girder near the bottom of the experimental cable as a reference, respectively. Stress was calculated from the strain data based on the calibration in the construction stage. The sampling frequencies of the GPS sensor and strain gauge are 1 Hz and 20 Hz, respectively. The GPS displacement of the tower and the stress of the girder are shown in Figure 15a,b, respectively.

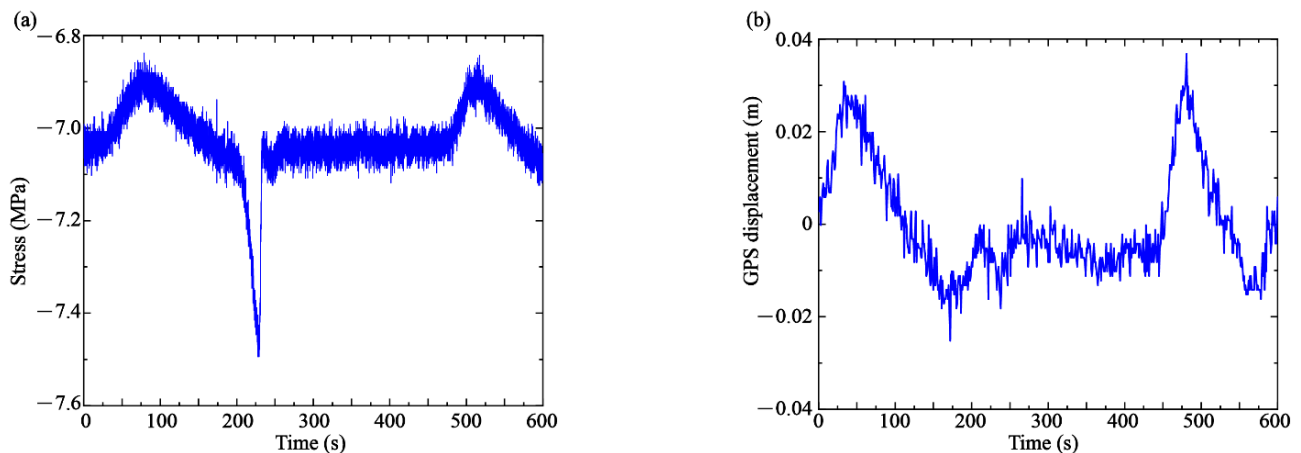


Figure 15. (a) The stress of the girder and (b) GPS displacement of the tower.

5.3. Identification Results and Discussion

The dynamic response was used to identify the tension based on the proposed algorithm. Firstly, the time-varying frequency of the acceleration signal was extracted using TFR techniques. The window function in STFT was also chosen as 256 based on the discussion in the workshop experiment. Moreover, the best identification range is between 5.0 to 7.0 Hz. Thus, the 15th, 16th, and 17th frequencies of cables were identified clearly from the reassignment spectrogram, as shown in Figure 16a. It is clear to see from Figure 16a that the structural frequency changes more frequently than the results of the workshop environment. Moreover, the identified time-varying frequency was used to calculate the tension by the 15th order frequency based on Equation (12), as shown in Figure 16b.

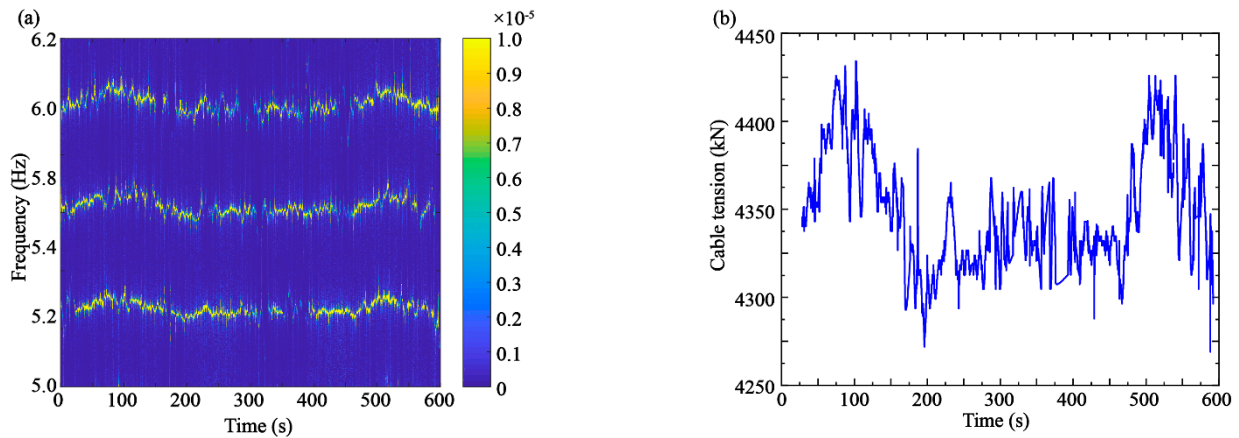


Figure 16. (a) TFR spectrogram of measured acceleration responses and (b) identified cable tension using 15th frequency.

The cable tension increased from 4325 ± 30 kN to 4425 ± 25 kN as the trucks moved over the bridge, as shown in Figure 16b. The tension variation was smaller than the truck’s static weight of 117.6 ± 3.92 kN because the loads were spread over two cables upstream and downstream. Moreover, the increasing moment of cable tension during Stage 1 in two cases coincided with the stress results, as shown in Figure 17a. The loading trucks passed through the mid-span area and moved to the South Tower during this period. Meanwhile, there was a sudden jump at about 200–225 s (Stage 2 in Case 1) when the trucks crossed the bottom region of the cable. The stress simultaneously decreased due to the compression of the steel box girder by the trucks. Therefore, the variation of identified tension is simultaneously changed with the stress of the girder. It is proved that the time-varying characteristics of cable tension can be extracted based on the proposed algorithm.

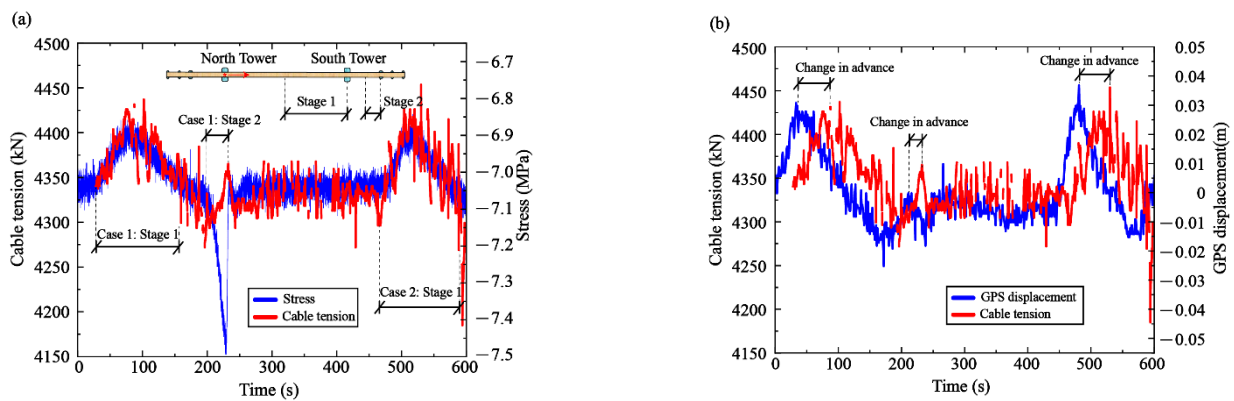


Figure 17. Comparison of cable tension to (a) stress and (b) GPS displacement.

For the GPS displacement shown in Figure 17b, there is still a high correlation between the GPS displacement and the trend of cable tension. However, the variation of GPS displacement was ahead of the identified tension because the displacement of the tower is a global parameter controlled by other cables. It can be found from the figure that the time to change in advance will be reduced as the truck gets closer to the location of the measured cable.

5.4. Assessment of Cable Tension

The identified time-varying tension can be used to assess the service performance of cables. The two indices are introduced to evaluate the operating condition of the measured cable, the 40% ultimate bearing tension, and the initial cable tension. The 40% ultimate bearing tension is the maximum allowable tension in the design stage to ensure

a safety coefficient within 2.5. The initial cable tension was measured when the bridge was completed in 2008. It is found in Figure 18a that the measured tension in the field experiment is between the middle of these two indices, 5732 kN and 4284 kN. There is still a large allowable range of cable tension under such a loading case.

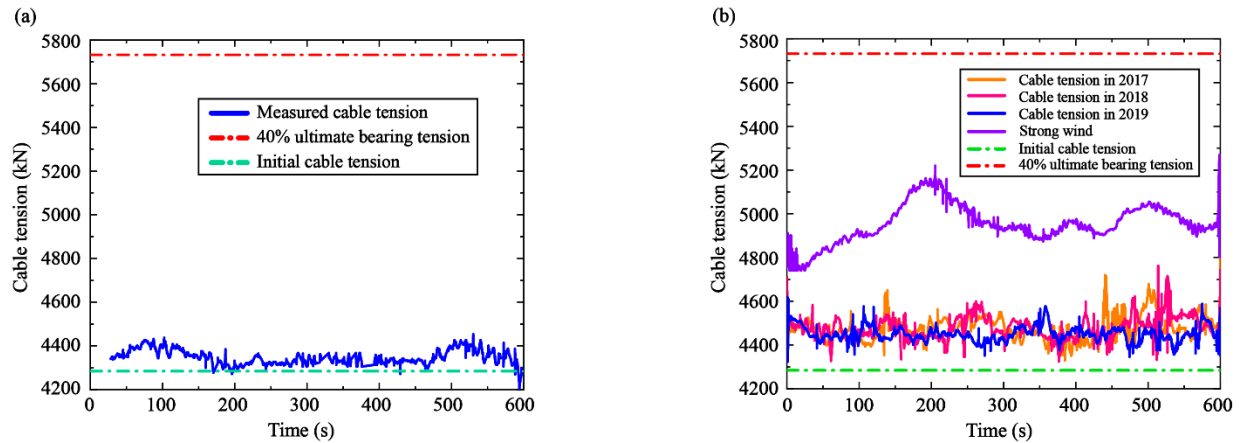


Figure 18. Assessment of service performance of the cable. (a) Results of the field experiment and (b) identified cable tension from 2017 to 2019 and an abnormal condition during strong winds.

The identified cable tension can also be used to reflect the deterioration or abnormal conditions of cables. Firstly, the time-varying tension is identified at 12 o'clock on March 31 from 2017 to 2019, as shown in Figure 18b. The identified tensions in 2017, 2018, and 2019 are marked with orange, pink and blue colors, respectively. The average values of these three years are all about 4500 ± 150 kN. The cable tension is mainly controlled by the moving loads. The operating condition of the cable is pretty healthy, and no obvious deterioration is found. Then, an abnormal condition is chosen to show the applications of the proposed algorithm during a strong wind in the summer of 2018, as marked with purple color in Figure 18b. The maximum wind speed at the height of the tower is more than 50 m/s during this server tropical storm. The cable tension increases to about 5100 ± 50 kN, much greater than the initial cable tension of 4284 kN. Fortunately, the cable tension remains within the designed 40% ultimate bearing tension of 5732 kN, showing that the service performance of the cable is under safety conditions.

6. Conclusions

In this study, the proposed TFR-based algorithm is proven to be effective in identifying time-varying cable tension, addressing the issue of insufficient efficiency and low resolution in the vibration-based method. Based on the results of the workshop tests and the dynamic experiment on the Sutong Bridge, the conclusions are remarked as follows:

- (1) The proposed algorithm can identify the time-varying instantaneously from reassignment spectrograms of acceleration responses. The measured time interval for the identification of frequency is within 12.8 s. Compared with the STFT results, the time-frequency resolution of the proposed algorithm is clear and has a satisfactory accuracy.
- (2) The experimental results show that the identification accuracy had a controllable error from the actual loads. The average error is between 0.16% and 0.59%, while the maximum error is 5.70%. The error usually appears at the boundary of the signals or calculated results by the low-order frequencies.
- (3) The identified tension has a synchronous trend with the adjacent structural responses, such as the GPS displacement of the tower and the stress of the girder. The identified results are consistent with the applied moving loads.
- (4) The proposed method can assess the deterioration or abnormal conditions of cables with two important indices, the 40% ultimate bearing tension and the initial cable tension measured in the construction stage.

For future research, the algorithm has potential application in the real-time structural health monitoring of the service performance of cables in extreme events, such as earthquakes, typhoons and accident predictions.

Author Contributions: Conceptualization, M.C. and X.Z.; methodology, S.H. and S.Z.; software, S.H.; validation, S.Z. and D.S.; writing—original draft preparation, S.H. and J.P.; writing—review and editing, M.C. and D.S.; project administration, X.Z.; funding acquisition, M.C. and X.Z. All authors have read and agreed to the published version of the manuscript.

Funding: This research was funded by the Anhui International Joint Research Center of Data Diagnosis and Smart Maintenance on Bridge Structures (No. 2021AHGHYB04), the Changzhou Policy Guidance Plan-International Science and Technology Cooperation Project (No. CZ20200003), the Nanjing Science and Technology Project (No. 202002014), and the Nantong Science and Technology Project (No. MS22021016).

Institutional Review Board Statement: Not applicable.

Informed Consent Statement: Not applicable.

Data Availability Statement: Not applicable.

Conflicts of Interest: The authors declare no conflict of interest.

References

1. Zhang, L.X.; Qiu, G.Y.; Chen, Z.S. Structural health monitoring methods of cables in cable-stayed bridge: A review. *Measurement* **2021**, *168*, 108343. [[CrossRef](#)]
2. Yang, Y.Q.; Fahmy, M.F.; Guan, S.J.; Pan, Z.H.; Zhan, Y.; Zhao, T.D. Properties and applications of FRP cable on long-span cable-supported bridges: A review. *Compos. Part B Eng.* **2020**, *190*, 107934. [[CrossRef](#)]
3. Wang, X.; Wu, Z.S. Integrated high-performance thousand-metre scale cable-stayed bridge with hybrid FRP cables. *Compos. Part B Eng.* **2010**, *41*, 166–175. [[CrossRef](#)]
4. Zhao, Y.B.; Sun, C.S.; Wang, Z.Q.; Wang, L.H. Analytical solutions for resonant response of suspended cables subjected to external excitation. *Nonlinear Dyn.* **2014**, *78*, 1017–1032. [[CrossRef](#)]
5. Khalifa, M.A.; Hodhod, O.A.; Zaki, M.A. Analysis and design methodology for an FRP cable-stayed pedestrian bridge. *Compos. Part B Eng.* **1996**, *27*, 307–317. [[CrossRef](#)]
6. Suzumura, K.; Nakamura, S. Environmental factors affecting corrosion of galvanized steel wires. *J. Mater. Civ. Eng.* **2004**, *16*, 1–7. [[CrossRef](#)]
7. Xia, Y.; Chen, B.; Weng, S.; Ni, Y.Q.; Xu, Y.L. Temperature effect on vibration properties of civil structures: A literature review and case studies. *J. Civ. Struct. Health* **2012**, *2*, 29–46. [[CrossRef](#)]
8. Zejli, H.; Gaillet, L.; Laksimi, A.; Benmedakhene, S. Detection of the presence of broken wires in cables by acoustic emission inspection. *J. Bridge Eng.* **2012**, *17*, 921–927. [[CrossRef](#)]
9. Li, R.; Miao, C.Q.; Feng, Z.X.; Wei, T.H. Experimental study on the fatigue behavior of corroded steel wire. *J. Constr. Steel Res.* **2021**, *176*, 106375. [[CrossRef](#)]
10. Xu, X.; Huang, Q.; Ren, Y.; Zhao, D.Y.; Zhang, D.Y.; Sun, H.B. Condition evaluation of suspension bridges for maintenance, repair and rehabilitation: A comprehensive framework. *Struct. Infrastruct. Eng.* **2019**, *15*, 555–567. [[CrossRef](#)]
11. Wang, H.; Tao, T.Y.; Li, A.Q.; Zhang, Y.F. Structural health monitoring system for Sutong cable-stayed bridge. *Smart Struct. Syst.* **2016**, *18*, 317–334. [[CrossRef](#)]
12. Li, S.L.; Li, H.; Liu, Y.; Lan, C.M.; Zhou, W.S.; Ou, J.P. SMC structural health monitoring benchmark problem using monitored data from an actual cable-stayed bridge. *Struct. Control Health Monit.* **2014**, *21*, 156–172. [[CrossRef](#)]
13. Peng, Z.; Li, J.; Hao, H. Long-term condition monitoring of cables for in-service cable-stayed bridges using matched vehicle-induced cable tension ratios. *Smart Struct. Syst.* **2022**, *29*, 167–179. [[CrossRef](#)]
14. Arangio, S.; Bontempi, F. Structural health monitoring of a cable-stayed bridge with Bayesian neural networks. *Struct. Infrastruct. Eng.* **2015**, *11*, 575–587. [[CrossRef](#)]
15. Cho, S.; Yim, J.; Shin, S.W.; Jung, H.J.; Yun, C.B.; Wang, M.L. Comparative field study of cable tension measurement for a cable-stayed bridge. *J. Bridge Eng.* **2013**, *18*, 748–757. [[CrossRef](#)]
16. Zheng, R.; Liu, L.H.; Zhao, X.; Chen, Z.Q.; Zhang, C.Y.; Hua, X.G. Investigation of measurability and reliability of adhesive-bonded built-in fiber Bragg grating sensors on steel wire for bridge cable force monitoring. *Measurement* **2018**, *129*, 349–357. [[CrossRef](#)]
17. Hu, D.T.; Guo, Y.X.; Chen, X.F.; Zhang, C.R. Cable force health monitoring of Tongwamen bridge based on fiber Bragg grating. *Appl. Sci.* **2017**, *7*, 384. [[CrossRef](#)]
18. Yim, J.; Wang, M.L.; Shin, S.W.; Yun, C.B.; Eem, S.H. Field application of elasto-magnetic stress sensors for monitoring of cable tension force in cable-stayed bridges. *Smart Struct. Syst.* **2013**, *12*, 465–482. [[CrossRef](#)]

19. Zhang, R.; Duan, Y.F.; Zhao, Y.; He, X. Temperature compensation of elasto-magneto-electric (EME) sensors in cable force monitoring using BP neural network. *Sensors* **2018**, *18*, 2176. [\[CrossRef\]](#)
20. Ma, L. A highly precise frequency-based method for estimating the tension of an inclined cable with unknown boundary conditions. *J. Sound Vib.* **2017**, *409*, 65–80. [\[CrossRef\]](#)
21. Zhang, X.; Peng, J.Y.; Cao, M.S.; Damjanović, D.; Ostachowicz, W. Identification of instantaneous tension of bridge cables from dynamic responses: STRICT algorithm and applications. *Mech. Syst. Signal Process.* **2020**, *142*, 106729. [\[CrossRef\]](#)
22. Fang, Z.; Wang, J.Q. Practical formula for cable tension estimation by vibration method. *J. Bridge Eng.* **2012**, *17*, 161–164. [\[CrossRef\]](#)
23. Kim, B.H.; Park, T. Estimation of cable tension force using the frequency-based system identification method. *J. Sound Vib.* **2007**, *304*, 660–676. [\[CrossRef\]](#)
24. Ren, W.X.; Chen, G.; Hu, W.H. Empirical formulas to estimate cable tension by cable fundamental frequency. *Struct. Eng. Mech.* **2005**, *20*, 363–380. [\[CrossRef\]](#)
25. He, W.Y.; Meng, F.C.; Ren, W.X. Cable force estimation of cables with small sag considering inclination angle effect. *Adv. Bridge Eng.* **2021**, *2*, 1–22. [\[CrossRef\]](#)
26. Zui, H.; Shinke, T.; Namita, Y. Practical formulas for estimation of cable tension by vibration method. *J. Struct. Eng.* **1996**, *122*, 651–656. [\[CrossRef\]](#)
27. Irvine, H.M. *Cable Structures*; The MIT Press: Cambridge, MA, USA, 1992.
28. Triantafyllou, M.S.; Grinfogel, L. Natural frequencies and modes of inclined cables. *J. Struct. Eng.* **1986**, *112*, 139–148. [\[CrossRef\]](#)
29. Wu, Q.X.; Takahashi, K.; Nakamura, S. Formulae for frequencies and modes of in-plane vibrations of small-sag inclined cables. *J. Sound Vib.* **2005**, *279*, 1155–1169. [\[CrossRef\]](#)
30. Li, H.; Zhang, F.J.; Jin, Y.Z. Real-time identification of time-varying tension in stay cables by monitoring cable transversal acceleration. *Struct. Control Health Monit.* **2014**, *21*, 1100–1117. [\[CrossRef\]](#)
31. Yang, Y.C.; Li, S.L.; Nagarajaiah, S.; Li, H.; Zhou, P. Real-time output-only identification of time-varying cable tension from accelerations via complexity pursuit. *J. Struct. Eng.* **2016**, *142*, 04015083. [\[CrossRef\]](#)
32. Bao, Y.Q.; Shi, Z.Q.; Beck, J.L.; Li, H.; Hou, T.Y. Identification of time-varying cable tension forces based on adaptive sparse time-frequency analysis of cable vibrations. *Struct. Control Health Monit.* **2017**, *24*, e1889. [\[CrossRef\]](#)
33. Liu, J.L.; Zheng, J.Y.; Wei, X.J.; Ren, W.X.; Laory, I. A combined method for instantaneous frequency identification in low frequency structures. *Eng. Struct.* **2019**, *194*, 370–383. [\[CrossRef\]](#)
34. Zhong, R.M.; Pai, P.F. An instantaneous frequency analysis method of stay cables. *J. Low Freq. Noise Vib. Act. Control* **2021**, *40*, 263–277. [\[CrossRef\]](#)
35. Hou, S.T.; Dong, B.; Fan, J.H.; Wu, G.; Wang, H.C.; Han, Y.T.; Zhao, X.J. Variational mode decomposition based time-varying force identification of stay cables. *Appl. Sci.* **2021**, *11*, 1254. [\[CrossRef\]](#)
36. Allen, J. Short term spectral analysis, synthesis, and modification by discrete Fourier transform. *IEEE Trans. Acoust. Speech Signal Process.* **1977**, *25*, 235–238. [\[CrossRef\]](#)
37. Hlawatsch, F.; Boudreaux-Bartels, G.F. Linear and quadratic time-frequency signal representations. *IEEE Signal Process. Mag.* **1992**, *9*, 21–67. [\[CrossRef\]](#)
38. Ribeiro, M.; Ewins, D.; Robb, D. Non-stationary analysis and noise filtering using a technique extended from the original prony method. *Mech. Syst. Signal Process.* **2003**, *17*, 533–549. [\[CrossRef\]](#)
39. Auger, F.; Flandrin, P. Improving the readability of time-frequency and time-scale representations by the reassignment method. *IEEE Trans. Signal Process.* **1995**, *43*, 1068–1089. [\[CrossRef\]](#)
40. Auger, F.; Flandrin, P.; Lin, Y.T.; McLaughlin, S.; Meignen, S.; Oberlin, T.; Wu, H.T. Time-frequency reassignment and synchrosqueezing: An overview. *IEEE Signal Process. Mag.* **2013**, *30*, 32–41. [\[CrossRef\]](#)
41. Chopra, A.K. *Dynamics of Structures*; Prentice Hall: Englewood Cliffs, NJ, USA, 2007.
42. You, Q.Z.; He, P.; Dong, X.W.; Zhang, X.G.; Wu, S.C. Sutong Bridge—The longest cable-stayed bridge in the world. *Struct. Eng. Int.* **2008**, *18*, 390–395. [\[CrossRef\]](#)